Theoretical Investigation of the Reaction of $CF_3CHFOCH_3$ with OH Radical

Hao Sun,[†,‡] Hongwei Gong,[§] Xiumei Pan,[†] Lizhu Hao,[||] ChiaChung Sun,[‡] Rongshun Wang,*[,†] and Xuri Huang*[,‡]

Institute of Functional Material Chemistry, Faculty of Chemistry, Northeast Normal University, Renmin Road 5268, Changchun, Jilin 130024, P.R. China, School of Public Health, Jilin University, Xinmin Street 1163, Changchun, Jilin 130021, P.R. China, Institute of Theoretical Chemistry, State Key Laboratory of Theoretical and Computational Chemistry, Jilin University, Changchun, Jilin Province 130023, P.R. China, and Key Laboratory for Applied Statistics of MOE (KLAS), School of Mathematics and Statistics, Northeast Normal University, Changchun, Jilin 130024, P.R. China

Received: January 21, 2009; Revised Manuscript Received: March 27, 2009

A direct ab initio dynamics method was used to study the mechanism and kinetics of the reaction $CF_3CHFOCH_3$ + OH. Two reaction channels, R1 and R2, were found, corresponding to H-abstraction from a $-CH_3$ group and a $-CHF$ group, respectively. The potential energy surface (PES) information was obtained at the G3(MP2)//MP2/6-311G(d,p) level. The standard enthalpies of formation for the reactant ($CF_3CHFOCH_3$) and products ($CF_3CHFOCH_2$ and CF_3CFOCH_3) were evaluated via isodesmic reactions at the same level. Furthermore, the rate constants of two channels were calculated using the canonical variational transition state theory (CVT) with small-curvature tunneling (SCT) contributions over a wide temperature range of 200−3000 K. The dynamic calculations demonstrate that reaction R1 dominates the overall reaction when the temperature is lower than 800 K whereas reaction R2 becomes more competitive in the higher temperature range. The calculated rate constants and branching ratios are both in good agreement with the available experimental values.

1. Introduction

Because they lack chlorine and bromine atoms in their molecules and have no potential for depleting ozone, hydrofluoroethers (HFEs) are currently used as third-generation substitutes for chlorofluorocarbons (CFCs) in foam-blowing and aerosol-propellant applications.[1−3] However, HFEs still have potential contributions to the greenhouse effect because of their strong absorption at 1000−3000 cm^{-1}.[4,5] To evaluate their environmental impact, the lifetimes of HFEs in the troposphere should be determined. Degradation of HFEs in the troposphere is mostly caused by hydroxyl radicals,[6] and therefore, much effort has been paid in recent years to the reactions of HFEs with hydroxyl radicals.[7−10]

For the title reaction, OH radicals can abstract hydrogen atoms both from $-CH_3$ groups and from $-CHF$ groups

$$CF_3CHFOCH_3 + OH \rightarrow CF_3CHFOCH_2 + H_2O \quad \text{(R1)}$$

$$\rightarrow CF_3CFOCH_3 + H_2O \quad \text{(R2)}$$

Chen et al.[7] measured a total rate constant of $(1.77 \pm 0.69) \times 10^{-12} \exp[(-720 \pm 110)/T]$ cm^3 $molecule^{-1}$ s^{-1} at 253−328 K. The rate constant was determined as $(1.56 \pm 0.06) \times 10^{-13}$ cm^3 $molecule^{-1}$ s^{-1}, and the competition ability (k_1/k_2) for reaction R1 and R2 was 4.2:1 at 298 K. To the best of our knowledge, little theoretical attention has been paid to this reaction, especially its kinetic properties over a wide temperature range. The present work focuses on the theoretical investigation of the mechanism and kinetics of the reaction of $CF_3CHFOCH_3$ with OH radical.

2. Computational Methods

Electronic structure calculations were carried out with the Gaussian 03 program suite.[11] The optimized geometries, harmonic vibrational frequencies, and zero-point energies (ZPEs) of all stationary points (reactants, complexes, transition states, and products) were calculated at the MP2/6-311G(d,p) level of theory.[12] The minimum-energy paths (MEPs) were obtained by intrinsic reaction coordinate (IRC) calculations[13−15] at the same levels. To acquire more reliable kinetic information, further single-point calculations were performed using the G3(MP2)[16] method with the MP2/6-311G(d,p)-optimized geometries. G3(MP2) is considered to be an efficient and economical method for calculating single-point energies of transient species involved in radical reactions, and in our previous reports,[17,18] we found the combination of MP2/6-311G(d,p) with G3(MP2) to accurately predict the reaction kinetics.

By means of the POLYRATE 8.4.1 program,[19] theoretical rate constants were calculated over the wide temperature range of 200−3000 K using the canonical variational transition state theory (CVT)[20−22] with the small-curvature tunneling (SCT) correction.[23,24] The potential energy surface information, including geometries, energies, gradients, and force constants of the stationary points and 24 extra points along the MEP, was obtained directly from electronic structure calculations. All vibrational modes, except for the lowest vibrational mode, were treated quantum mechanically as separable harmonic oscillators,

* To whom correspondence should be addressed. E-mail: wangrs@nenu.edu.cn (R.W.), huangxr@mail.jlu.edu.cn (X.H.). Tel.: +86-431-85099511. Fax: +86-431-85099511.
† Faculty of Chemistry, Northeast Normal University.
‡ State Key Laboratory of Theoretical and Computational Chemistry, Jilin University.
§ School of Public Health, Jilin University.
|| School of Mathematics and Statistics, Northeast Normal University.

10.1021/jp9006262 CCC: $40.75 © 2009 American Chemical Society
Published on Web 04/27/2009

TABLE 1: Calculated Vibrational Frequencies (in cm^{-1}) and $\langle S^2 \rangle$ Values of the Stationary Points at the MP2/6-311G(d,p) Level for the Reaction $CF_3CHFOCH_3 + OH$

species	frequencies	$\langle S^2 \rangle$
$CF_3CHFOCH_3$	72, 87, 157, 189, 245, 344, 371, 411, 535, 586, 616, 733, 909, 1053, 1100, 1183, 1201, 1233, 1253, 1277, 1348, 1415, 1493, 1510, 1516, 1538, 3069, 3094, 3162, 3220	0.0
OH	3855	0.755
CF_3CFOCH_3	60, 79, 155, 173, 244, 318, 372, 417, 530, 589, 649, 731, 865, 1028, 1148, 1196, 1211, 1227, 1267,1313, 1466, 1515, 1523, 1532, 3098, 3193, 3233	0.757
$CF_3CHFOCH_2$	73, 97, 181, 237, 251, 351, 376, 412, 534, 586, 615, 734, 745, 909, 1091, 1119, 1203, 1241, 1260, 1284, 1350, 1413, 1498, 1511, 3134, 3196, 3352	0.760
H_2O	1668, 3906, 4013	0.0
TS1	−1810, 26, 72, 103, 152, 176, 250, 304, 333, 370, 378, 412, 536, 585, 622, 731, 788, 912, 926, 1056, 1102, 1158, 1215, 1238, 1257, 1265, 1352, 1405, 1436, 1501, 1504, 1532, 3130, 3155, 3232, 3827	0.777
TS2	−1912, 57, 86, 109, 119, 165, 183, 206, 251, 338, 370, 407, 468, 569, 590, 634, 755, 852, 980, 1041, 1119, 1182, 1206, 1236, 1266, 1293, 1307, 1447, 1511, 1517, 1535, 1541, 3094, 3188, 3229, 3835	0.776
COMR1	34, 54, 83, 92, 135, 158, 191, 253, 273, 347, 371, 407, 416, 535, 586, 609, 734, 911, 1040, 1065, 1185, 1199, 1234, 1255, 1285, 1347, 1421, 1491, 1508, 1521, 1537, 3080, 3128, 3170, 3222, 3825	0.755
COMP1	52, 60, 78, 102, 126, 141, 194, 216, 247, 289, 340, 356, 379, 412, 533, 586, 607, 632, 735, 914, 1080, 1102, 1204, 1241, 1257, 1292, 1354, 1425, 1501, 1518, 1658, 3166, 3198, 3364, 3887, 4000	0.761
COMP2	39, 50, 94, 108, 119, 169, 177, 199, 242, 245, 319, 360, 374, 417, 530, 588, 650, 731, 863, 1011, 1132, 1203, 1211, 1229, 1264, 1321, 1472, 1522, 1533, 1543, 1682, 3106, 3207, 3239, 3891, 3990	0.757

whereas for the lowest-frequency mode, the partition function was evaluated by the hindered-rotor approximation of Truhlar and Chuang.[25,26] During the kinetic calculations, the Euler single-step integrator with a step of 0.001 $(amu)^{1/2}$ bohr was used to follow the MEP, generalized normal-mode analysis was performed at 0.01 $(amu)^{1/2}$ bohr. In the calculation of the electronic partition functions, the two electronic states of the OH radicals were included, with a 140 cm^{-1} (637.882×10^{-6} hartree) splitting in the $^2\Pi$ ground state. The curvature components were calculated using a quadratic fit to obtain the derivative of the gradient with respect to the reaction coordinate. The total rate constant was obtained as the sum of the individual rate constants associated with reactions R1 and R2. Furthermore, the branching ratios of reactions R1 and R2, k_1/k and k_2/k, respectively, were also calculated.

The major problem in applying the unrestricted spin formalism is contamination with higher spin states. Severe spin contamination could lead to a worse estimation of the barrier height.[27,28] We examined the spin contamination before and after annihilation for all species involved in the title reaction. Table 1 shows that the $\langle S^2 \rangle$ values for the doublet range from 0.755 to 0.777 before annihilation, whereas after annihilation, $\langle S^2 \rangle$ is 0.75 (the exact value for a pure doublet), with a maximum difference of 4.67%, less than the permitted criterion of 10%.[29] Consequently, the wave function was not severely contaminated by states of higher multiplicity.

3. Results and Discussion

3.1. Reaction Mechanism. The optimized geometries of the reactants, complexes, saddle points, and products are shown in Figure 1. In fact, several different conformations of the $CF_3CHFOCH_3$ molecule exist, and it was important to locate the most stable one as the starting geometry of the reactant for our calculations. The conformation with an anti-COC′C framework is known to have the lowest energy. Therefore, our analysis focused on the rotations of C—O and C′—C bonds. The scanning calculation was performed to investigate the effects of C—O and C′—C rotations on the $CF_3CHFOCH_3$ energy, with dihedral angles H(1)COC′and F′CC′O ranging from −179° to 180°. The calculations showed that $CF_3CHFOCH_3$ is the most stable when dihedral angle H(1)COC′ equals −70°, 50°, or 170° and dihedral angle F′CC′O is −60°, 60°, or 180°, and therefore, such a stable conformation was used as starting point in the subsequent optimization. Some typical curves of the dependence of the $CF_3CHFOCH_3$ energy on C—O and C′—C rotations are depicted in Figure 2. Table 1 lists the harmonic vibrational frequencies of all of the stationary points calculated at the MP2/6-311G(d,p) level. The reactants, complexes, and products correspond to all-real frequencies, and the transition states are confirmed to have only one imaginary vibrational frequency. Table 2 lists the calculated relative energies (E_{rel}), reaction enthalpies ($\Delta H^0_{r,298}$), and C—H bond dissociation energies (D^0_{298}) of $CF_3CHFOCH_3$. It is worth noticing that the loose geometries of the complexes have low relative energies in Figure 1. PMP2 relative energies are listed in Table 1 to further reveal the effects of spin contamination on the calculated energies. As can be seen in Table 1, the differences between the PMP2 and MP2 energies are very small, which also confirms that the computational wave function is proper for the title reaction system. We speculate that intramolecular hydrogen bonds stabilize the complexes and loosen their geometries at the same time. The profile of the potential energy surface obtained at the G3(MP2)//MP2/6-311G(d,p) is depicted in Figure 3. The energies used in the discussion correspond to the G3(MP2)//MP2/6-311G(d,p) level with ZPE corrections at the MP2/6-311G(d,p) level, unless otherwise stated.

Because the three hydrogen atoms of the $-CH_3$ group in the $CF_3CHFOCH_3$ molecule are equivalent, only one channel is feasible for reaction R1. Complexes COMR1 and COMP1 are located in the entrance and exit valleys, respectively, and their energies are 0.87 and 21.19 kcal/mol lower than that of the reactant. The H(1)—O bond distance in COMR1 is 3.021 Å, and the H(1)—C bond distance in COMP1 is 2.657 Å. In the saddle point, TS1, the lengths of the breaking C—H bond and

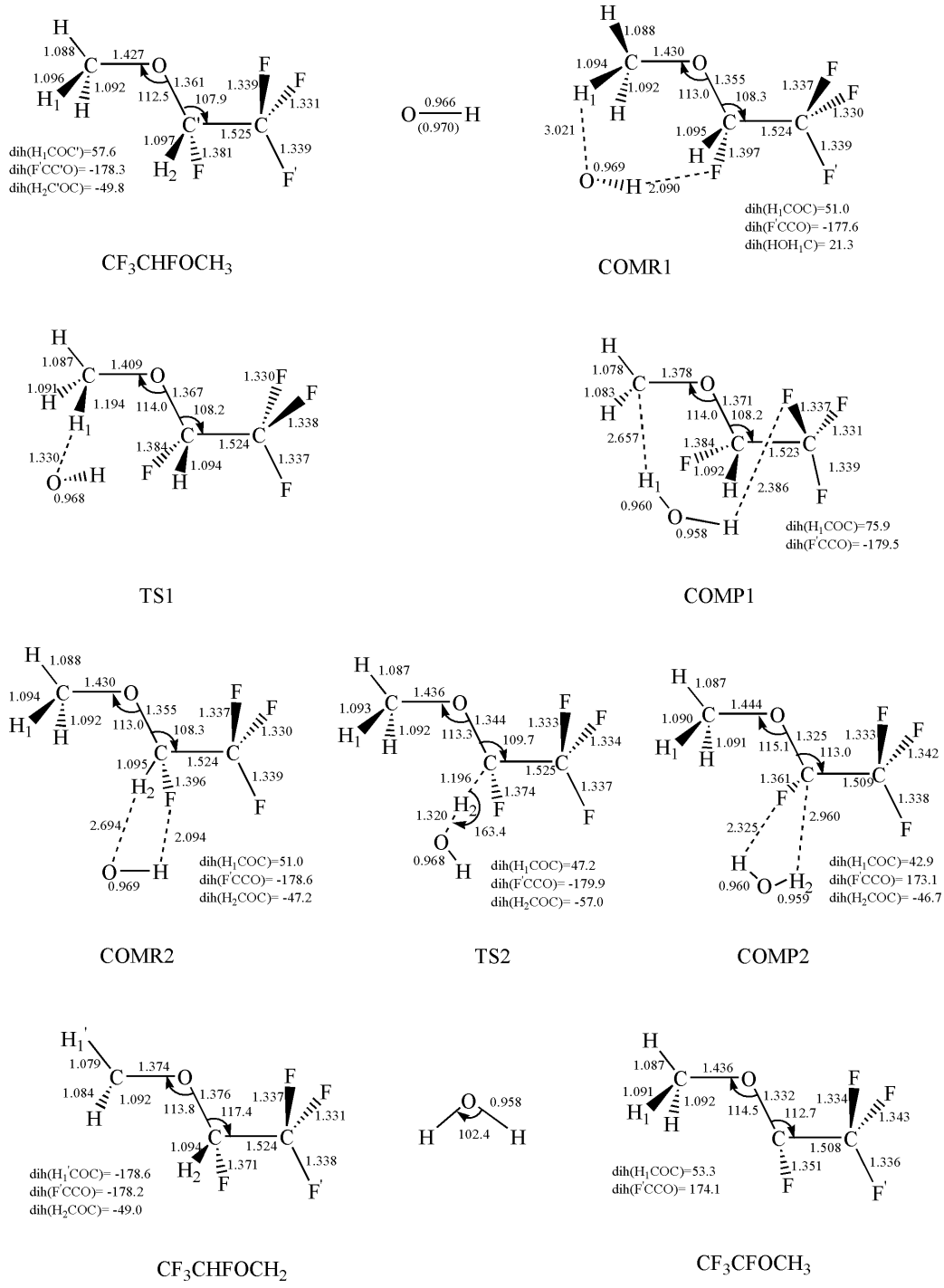

Figure 1. Optimized geometries (bond lengths in angstrom and angles in degree) of all stationary points at the MP2/6-311G(d,p) level.

the newly formed H—O bond are 1.194 and 1.330 Å, respectively, which are 8.9% and 38.8% longer than the corresponding equilibrium bond lengths of C—H in $CF_3CHFOCH_3$ and H—O in H_2O. Consequently, TS1 can be considered as an early barrier. As seen in Table 2, this early or late character in the transition states is in keeping with the perspective of Fisher and Radom[30] that an endothermic reaction proceeds via a "late" transition state whereas an exothermic reaction corresponds to an "early" transition state. Finally, P1, $CF_3CHFOCH_2 + H_2O$, is generated, and the reaction enthalpy ($\Delta H^0_{r,298}$) for R1 is −17.50 kcal/mol.

Similarly to channel R1, there exist complexes at the entrance and exit of channel R2. COMR2 and COMP2 have relative energies of −0.90 and −18.36 kcal/mol, respectively. The bond lengths of H(2)—O in COMR2 and H(2)—C in COMP2 are 2.694 and 2.960 Å, respectively. In the TS2 structure, the breaking C—H bond is 1.196 Å, stretched by 9.0%, and the newly formed H—O bond is 1.320 Å, 37.8% longer than the equilibrium bond length in HCl, indicating that reaction R2 also occurs via an early barrier. From Table 2, the exothermicity and early property of the barrier for reaction R2 also follow Fisher and Radom's general rule. The products of reaction R2 are $CF_3CFOCH_3 + H_2O$, and 16.66 kcal/mol of heat is released.

Table 2 also lists the C—H bond dissociation energies (D^0_{298}) of CF_3CFOCH_3. The calculated C—H D^0_{298} values for the —CH_3 and —CHF groups at the G3(MP2)//MP2/6-311G(d,p) level are 97.11 and 97.84 kcal mol^{-1}, respectively. From a comparison of the heights of the energy barriers, reaction enthalpies of the two channels, and C—H bond dissociation energies of the —CH_3

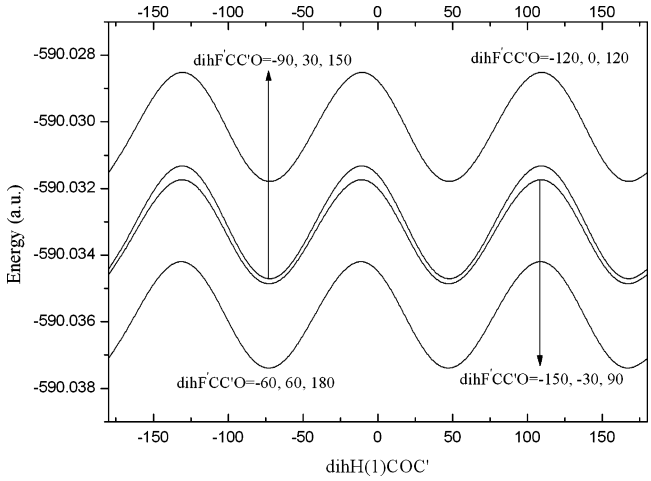

Figure 2. Scans of the dependence of the $CF_3CHFOCH_3$ energy on C—O and C′—C rotations (angles in degree).

TABLE 2: Calculated Reaction Enthalpies ($\Delta H^0_{r,298}$, kcal/mol) for Two Reaction Channels and Dissociation Energy of C—H bonds (D^0_{298}, kcal/mol) in $CF_3CHFOCH_3$ at the MP2/6-311G(d,p) and G3(MP2)//MP2/6-311G(d,p) Levels[a]

	MP2	PMP2	G3(MP2)// MP2
E_{rel}			
R: $CF_3CHFOCH_3$ + OH	0.0	0.0	0.0
COMR1	−3.91	−3.92	−0.87
TS1	4.86	3.91	4.12
COMP1	−23.46	−23.65	−21.19
P1: $CF_3CHFOCH_2$ + H_2O	−17.90	−18.02	−17.50
COMR2	−3.92	−3.93	−0.90
TS2	5.85	4.98	5.03
COMP2	−21.64	−21.54	−18.36
P2: CF_3CFOCH_3 + H_2O	−17.06	−16.94	−17.00
$\Delta H^0_{r,298}$			
R1	−17.66		−17.50
R2	−16.72		−16.66
D^0_{298}			
$CF_3CHFOCH_3 \rightarrow CF_3CHFOCH_2$ + H	93.93		97.11
$CF_3CHFOCH_3 \rightarrow CF_3CFOCH_3$ + H	94.77		97.84

[a] All values obtained at the MP2/6-311G(d,p) and G3(MP2) levels with ZPE or TZPE corrections of the lower level (in units of kcal/mol).

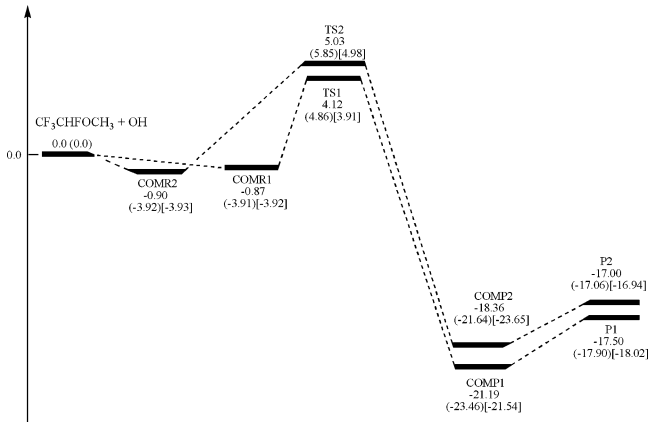

Figure 3. Schematic potential energy surface for the $CF_3CHFOCH_3$ + OH reaction obtained at the G3(MP2)//MP2/6-311G(d,p) level. The values in parentheses and brackets are MP2 and PMP2 energies, respectively (energies in kcal/mol).

and CHF groups, we can speculate that channel R1 is the dominant channel of the overall reaction. This view is further supported by the rate-constant study reported in section 3.2.2.

3.2. Calculations of Standard Enthalpies of Formation. Accurate thermodynamic values are important in evaluating the environmental impact of atmospheric species. The standard enthalpies of formation for many HFE molecules, such as $CHF_2OCF_2CHF_2$, $CH_3OCF_2CHF_2$, and $CH_3OCH_2CHF_2$, have been calculated theoretically.[31] Because little has been reported on the energetics of the species involved in the title reaction, $CF_3CHFOCH_3$, $CF_3CHFOCH_2$, and CF_3CFOCH_3, we performed calculations at the G3(MP2)//MP2/6-311G(d,p) to predict the enthalpies of formation of these three species using the following isodesmic reactions

$$CF_3CHFOCH_3 + CH_2F_2 \rightarrow CH_3OCH_3 + CF_3CF_3 \quad \text{(R3a)}$$

$$CF_3CHFOCH_3 + H_2O + CH_4 \rightarrow CH_3OH + CH_3OH + CF_3CH_2F \quad \text{(R3b)}$$

$$CF_3CHFOCH_3 + CH_3F \rightarrow CF_3CF_2OCH_3 + CH_4 \quad \text{(R3c)}$$

$$CF_3CHFOCH_2 + CH_4 \rightarrow CH_3OCH_3 + CHFCF_3 \quad \text{(R4a)}$$

$$CF_3CHFOCH_2 + H_2O + CH_4 \rightarrow CH_3OH + CH_3OH + CHFCF_3 \quad \text{(R4b)}$$

$$CF_3CHFOCH_2 + CH_2O + CH_4 \rightarrow CH_3OCH_3 + HCO + CF_3CH_2F \quad \text{(R4c)}$$

$$CF_3CFOCH_3 + CH_4 \rightarrow CH_3OCH_3 + CHFCF_3 \quad \text{(R5a)}$$

$$CF_3CFOCH_3 + H_2O + CH_4 \rightarrow CH_3OH + CH_3OH + CF_3CHF \quad \text{(R5b)}$$

$$CF_3CFOCH_3 + CH_2O + CH_4 \rightarrow CH_3OCH_3 + HCO + CF_3CH_2F \quad \text{(R5c)}$$

The enthalpies of formation of all species involved in reactions R3a−R5c, except $CF_3CHFOCH_3$, $CF_3CHFOCH_2$, and CF_3CFOCH_3, have been reported (CH_2F_2, −108.2 ± 0.2 kcal/mol;[32a] CH_3OCH_3, −44.0 ± 0.1 kcal/mol;[32b] CF_3CF_3, −320.89 kcal/mol;[32c] H_2O, −57.798 ± 0.01 kcal/mol;[32d] CH_4, −17.80 ± 0.10 kcal/mol;[32b] CH_3OH, −48.04 ± 0.14 kcal/mol;[32e] CF_3CH_2F, −214.1 ± 2 kcal/mol;[32c] CH_3F, −56.8 ± 2 kcal/mol;[32f] $CF_3CF_2OCH_3$, −316.92 kcal/mol;[31] $CHFCF_3$, −166.5 kcal/mol;[32f] CH_2O, −25.98 ± 0.01 kcal/mol;[32e] HCO, 10.55 ± 0.10 kcal/mol[32e]). The reaction enthalpies of reactions R3a−R5c were calculated at the G3(MP2)//MP2/6-311G(d,p) level, so that the enthalpies of formation of $CF_3CHFOCH_3$, $CF_3CHFOCH_2$, and CF_3CFOCH_3 could be obtained using these isodesmic reactions. As listed in Table 3, the average values of the enthalpies of formation were also calculated to ensure accuracy. The enthalpies of formation of $CF_3CHFOCH_3$, $CF_3CHFOCH_2$, and CF_3CFOCH_3 were found to be −257.23, −208.55, and −207.71 kcal/mol, respectively. Such calculations provide valuable information for thermochemical databases.

3.2. Dynamic Calculations. ***3.2.1. Reaction-Path Properties.*** The calculation results demonstrate that reactions R1 and R2 have similar characters, and therefore, we give an example of reaction R2 to illuminate the reaction-path properties of the title reaction in this section. Figure 4 shows the classical potential energy (V_{MEP}), the ground-state vibrational adiabatic

TABLE 3: Calculated Enthalpies of Formation (kcal/mol) of $CF_3CHFOCH_3$, $CF_3CHFOCH_2$, and CF_3CFOCH_3

species	isodesmic reaction	MP2 $\Delta H^0_{f,298}$	MP2 average	G3(MP2) $\Delta H^0_{f,298}$	G3(MP2) average
$CF_3CHFOCH_3$	*R3a*	−254.10	−255.66	−256.22	−257.23
	R3b	−254.92		−254.81	
	R3c	−257.95		−260.65	
$CF_3CHFOCH_2$	*R4a*	−210.82	−212.43	−209.70	−208.55
	R4b	−210.35		−210.04	
	R4c	−205.26		−205.92	
CF_3CFOCH_3	*R5a*	−209.88	−207.87	−208.86	−207.71
	R5b	−209.41		−209.20	
	R5c	−204.31		−205.08	

potential energy (V_a^G), and the zero-point energy (ZPE) for reaction R2 as functions of the intrinsic reaction coordinate (s) at the G3(MP2)//MP2/6-311G(d,p) level, where $V_a^G = V_{MEP}$ + ZPE. From Figure 4, the coincidence of the maxima of the V_{MEP} and V_a^G curves implies a small variational effect for reaction R2. Reaction R1 also exhibits features similar to those of reaction R2.

Figure 5 depicts the variation of the generalized normal-mode vibrational frequencies along the MEP for reaction R2. In the negative limit of s, the frequencies are associated with those of the reactant complex, and in the positive limit of s, they correspond to those of the products, H_2O and CF_3CFOCH_3. In the process of the reaction, most of those frequencies do not change significantly on going from the reactants to the products. However, mode 1 (the bold line in Figure 5), which connects the stretching vibrational mode of the breaking and forming bonds, exhibits a dramatic drop in the s range from −0.45 to 0.63 $(amu)^{1/2}$ bohr. Therefore, mode 1 is referred to as the "reactive mode". This kind of mode is known to be the typical character of hydrogen-transfer reaction.[33]

3.2.2. Rate-Constant Calculations. On the basis of the G3(MP2)//MP2/6-311G(d,p) PES information, direct dynamics calculations for $CF_3CHFOCH_3$ + OH reaction were carried out using variational transition state theory with interpolated single-point energies. The CVT/SCT rate constants were calculated over the temperature range of 200−3000 K. The total rate constant was determined as the sum of the individual rate constants of the two channels, i.e., $k = k_1 + k_2$. Plots of the calculated rate constants are shown in Figure 6. To reveal

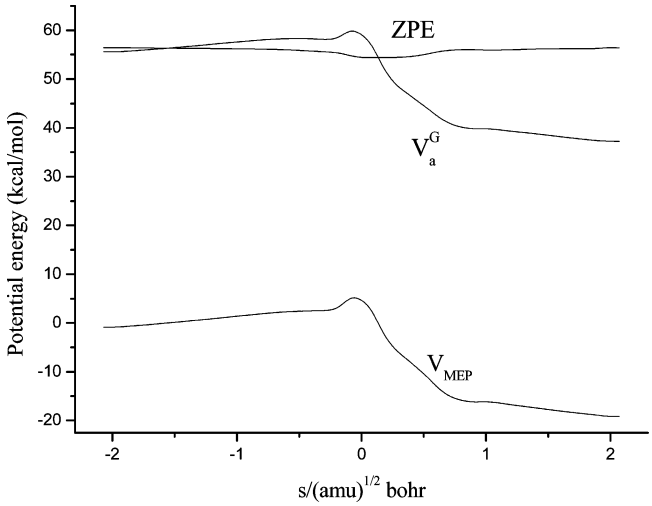

Figure 4. Classical potential energy curve (V_{MEP}), ground-state vibrationally adiabatic energy curve (V_a^G), and zero-point energy (ZPE) curve as functions of s $(amu)^{1/2}$ bohr at the G3(MP2)//MP2/6-311G(d,p) level for reaction R2.

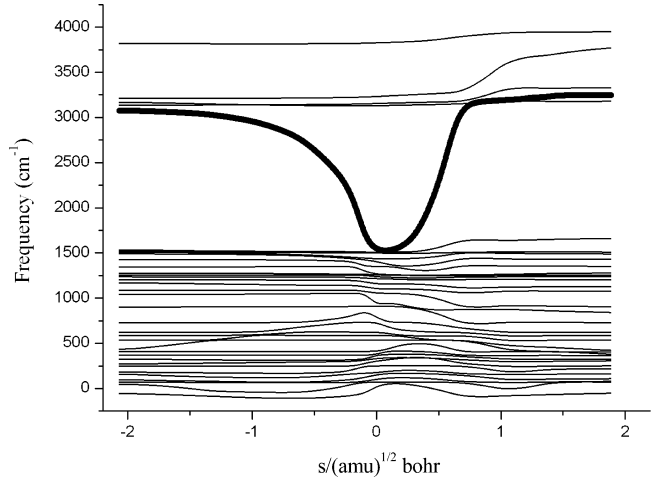

Figure 5. Changes of the generalized normal-mode vibrational frequencies as functions of s $(amu)^{1/2}$ bohr at the G3(MP2)//MP2/6-311G(d,p) level for reaction R2.

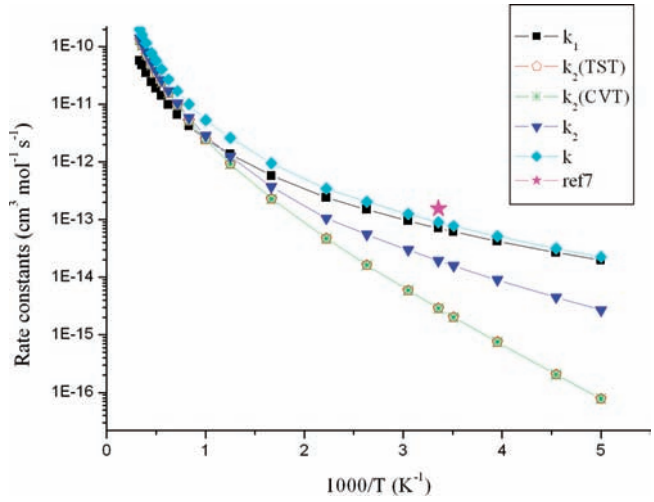

Figure 6. Calculated rate constants at the G3(MP2)//MP2/6-311G(d,p) level between 200 and 3000 K for the $CF_3CHFOCH_3$ + OH reaction, along with the available experimental value.

the variational and tunneling contributions to rate constants calculations, Figure 6 also includes the curves for the TST and CVT rate constants of reaction R2.

Figure 6 shows that the CVT and TST rate constants for reaction R2 are almost superposed on each other over the whole temperature range, suggesting that the variational effects can be neglectable. However, deviations between the CVT and CVT/SCT rate constants are notable over the temperature range of 200−600 K, implying that the tunneling contribution plays an important role in calculations of the rate constants at low temperatures. The small-curvature effect is significant in the title reaction, and hence, a noticeable curvature can be expected in the Arrhenius plot. Figure 6 also shows that the calculated rate constant (9.01×10^{-14} cm^3 molecule^{-1} s^{-1} at 298 K) is in good agreement with the available experimental value [$(1.56 \pm 0.06) \times 10^{-13}$ cm^3 molecule^{-1} s^{-1}]. In addition, it can be seen from Figure 6 that the rate constants for the $CF_3CHFOCH_3$ + OH reaction are small at lower temperatures but increase rapidly as temperature rises. Therefore, the reaction might have some effect on the atmosphere under high-temperature conditions.

Figure 7 depicts the temperature dependence of the branching ratios, k_1/k and k_2/k. The calculated value of k_1/k (0.785) at 298 K agrees well with the experimental value of 0.808.[7] The competition of reactions R1 and R2 can also be observed from

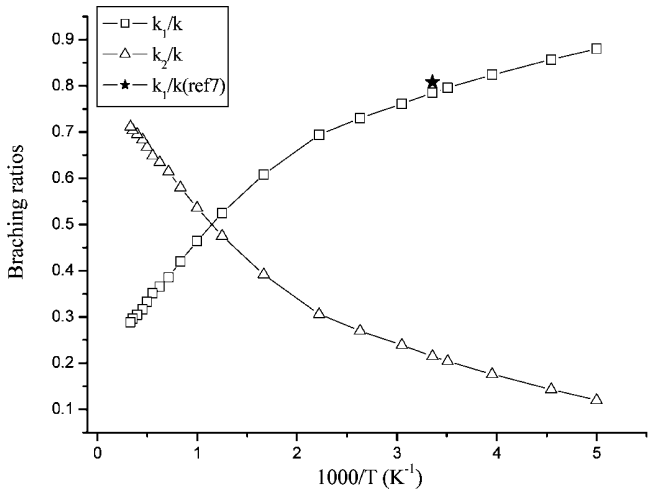

Figure 7. Calculated and experimental branching ratios for the $CF_3CHFOCH_3 + OH$ reaction as functions of $1000/T$ between 200 and 3000 K at the G3(MP2)//MP2/6-311G(d,p) level.

Figure 7. In the low-temperature range, channel R1 exhibits significant predominance, but its preponderance is gradually weakened as the temperature increases. Because k_1/k decreases to 0.525 when the temperature reaches 800 K, it is reasonable to deduce that channel R2 should dominate the overall reaction as the temperature increases further.

Because of the lack of experimental data over a wide temperature range, the CVT/SCT rate constants of each channel and the overall reaction over the temperature range of 200−3000 K, fitted by three-parameter formulas, are given as follows (in cm^3 $molecule^{-1}$ s^{-1})

$$k_1 = (3.26\times10^{-21})T^{2.98}\exp(-26.94/T)$$

$$k_2 = (3.70\times10^{-22})T^{3.34}\exp(-384.73/T)$$

$$k = (6.66\times10^{-22})T^{3.31}\exp(-41.08/T)$$

4. Conclusions

The hydrogen-abstraction reaction $CF_3CHFOCH_3 + OH$ was investigated by a direct ab initio dynamics method at the G3(MP2)//MP2/6-311G (d,p) level. Hydrogen abstractions from the $-CH_3$ and $-CHF$ groups were found to be feasible, and two corresponding transition states were located. The standard enthalpies of formation of $CF_3CHFOCH_3$, $CF_3CHFOCH_2$, and CF_3CFOCH_3 were calculated to be −257.23, −208.55, and −207.71 kcal/mol, respectively, using the isodesmic reaction model. The rate constants were calculated by canonical variational transition state theory (CVT) with the small-curvature tunneling (SCT) correction over the temperature range of 200−3000 K. The calculations showed that the variational effect is negligible for the title reaction and small-curvature tunneling is significant for calculating the rate constants at lower temperatures. The calculated rate constant and branching ratio at 298 K are in good agreement with the available experimental values. The dynamics calculations also indicate that channel R1 dominates the title reaction from 200 to 800 K whereas the reaction proceeds mainly via channel R2 at temperatures higher than 800 K.

Acknowledgment. The authors thank Professor Donald G. Truhlar for providing the POLYRATE 8.4.1 program. This work was supported by the National Natural Science Foundation of China (Nos. 20773048 and 20773021). We are greatly thankful for the referees' helpful comments.

References and Notes

(1) Tsai, W. T. *J. Hazard. Mater.* **2005**, *119*, 69.
(2) Sekiya, A.; Misaki, S. *J. Fluorine Chem.* **2000**, *101*, 215.
(3) Bivens, D. B.; Minor, B. H. *Int. J. Refrig.* **1998**, *21*, 567.
(4) Imasu, R.; Suga, A.; Matsuno, T. *J. Meteorol. Soc. Jpn.* **1995**, *73*, 1123.
(5) Houghton, J. T.; Ding Y.; Griggs, D. J.; Noguer, M.; van der Linden, P. J.; Dai, X.; Maskell, K.; Johnson, C. A. *Climate Change, 2001: The Scientific Basis. Contribution of Working Group I to the Third Assessment Report of the Intergovernmental Panel on Climate Change*; Intergovernmental Panel on Climate Change (IPCC): Geneva, Switzerland, 2001.
(6) Wallington, T. J.; Schneider, W. F.; Sehested, J.; Bilde, M.; Platz, J.; Nielsen, O. J.; Christensen, L. K. *J. Phys. Chem. A* **1997**, *101*, 8264.
(7) Chen, L.; Kutsuna, S.; Tokuhashi, K.; Sekiya, A. *J. Phys. Chem. A* **2006**, *110*, 12845.
(8) Urata, S.; Takada, A.; Uchimaru, T.; Chandra, A. K. *Chem. Phys. Lett.* **2003**, *368*, 215.
(9) Fontana, G.; Gausa, M.; Gianotti, V.; Marchionni, G. *J. Fluorine Chem.* **2001**, *109*, 113.
(10) Chen, L.; Kutsuna, S.; Tokuhashi, K.; Sekiya, A.; Takeuchi, K.; Ibusuki, T. *Int. J. Chem. Kinet.* **2003**, *35*, 239.
(11) Frisch, M. J.; Trucks, G. W.; Schlegel, H. B.; Scuseria, G. E.; Robb, M. A.; Cheeseman, J. R.; Montgomery, J. A., Jr.; Vreven, T.; Kudin, K. N.; Burant, J. C.; Millam, J. M.; Iyengar, S. S.; Tomasi, J.; Barone, V.; Mennucci, B.; Cossi, M.; Scalmani, G.; Rega, N.; Petersson, G. A.; Nakatsuji, H.; Hada, M.; Ehara, M.; Toyota, K.; Fukuda, R.; Hasegawa, J.; Ishida, M.; Nakajima, T.; Honda, Y.; Kitao, O.; Nakai, H.; Klene, M.; Li, X.; Knox, J. E.; Hratchian, H. P.; Cross, J. B.; Bakken, V.; Adamo, C.; Jaramillo, J.; Gomperts, R.; Stratmann, R. E.; Yazyev, O.; Austin, A. J.; Cammi, R.; Pomelli, C.; Ochterski, J. W.; Ayala, P. Y.; Morokuma, K.; Voth, G. A.; Salvador, P.; Dannenberg, J. J.; Zakrzewski, V. G.; Dapprich, S.; Daniels, A. D.; Strain, M. C.; Farkas, O.; Malick, D. K.; Rabuck, A. D.; Raghavachari, K.; Foresman, J. B.; Ortiz, J. V.; Cui, Q.; Baboul, A. G.; Clifford, S.; Cioslowski, J.; Stefanov, B. B.; Liu, G.; Liashenko, A.; Piskorz, P.; Komaromi, I.; Martin, R. L.; Fox, D. J.; Keith, T.; Al-Laham, M. A.; Peng, C. Y.; Nanayakkara, A.; Challacombe, M.; Gill, P. M. W.; Johnson, B.; Chen, W.; Wong, M. W.; Gonzalez, C.; Pople, J. A. *Gaussian 03*, revision C.02; Gaussian, Inc.: Wallingford, CT, 2004.
(12) Head-Gordon, M.; Pople, J. A.; Frisch, M. J. *Chem. Phys. Lett.* **1988**, *153*, 503.
(13) Fukui, K.; Kato, S.; Fujimoto, H. *J. Am. Chem. Soc.* **1975**, *97*, 1.
(14) Gonzalez, C.; Schlegel, H. B. *J. Chem. Phys.* **1989**, *90*, 2154.
(15) Gonzalez, C.; Schlegel, H. B. *J. Phys. Chem.* **1990**, *94*, 5523.
(16) Curtiss, L. A.; Redfern, P. C.; Raghavachari, K.; Rassolov, V.; Pople, J. A. *J. Chem. Phys.* **1999**, *110*, 4703.
(17) Sun, H.; He, H. Q.; Liu, J. Y.; Li, Z. S.; Pan, X. M.; Wang, R. S. *ChemPhysChem* **2008**, *9*, 847.
(18) Sun, H.; Huang, X. R.; Pan, X. M.; Wang, R. S.; Sun, C. C. *Int. J. Chem. Kinet.* **2009**, *41*, 394–400.
(19) Chuang, Y. Y.; Corchado, J. C.; Fast, P. L.; Villa, J.; Hu, W. P.; Liu, Y. P.; Lynch; G. C.; Jackels, C. F.; Nguyen, K. A.; Gu; M. Z.; Rossi, I.; Coitino; E. L.; Clayton, S.; Melissas, V. S.; Lynch; B. J.; Steckler, R.; Garrett, B. C.; Isaacson, A. D.; Truhlar, D. G. *POLYRATE*, version 8.4.1; University of Minnnesota: Minneapolis, MN, 2000.
(20) Garrett, B. C.; Truhlar, D. G. *J. Am. Chem. Soc.* **1979**, *101*, 4534.
(21) Garrett, B. C.; Truhlar, D. G.; Grev, R. S.; Magnuson, A. W. *J. Phys. Chem.* **1980**, *84*, 1730.
(22) Garrett, B. C.; Truhlar, D. G. *J. Chem. Phys.* **1979**, *70*, 1593.
(23) Liu, Y. P.; Lynch, G. C.; Truong, T. N.; Lu, D. H.; Truhlar, D. G.; Garrett, B. C. *J. Am. Chem. Soc.* **1993**, *115*, 2408.
(24) Lu, D. H.; Truong, T. N.; Melissas, V. S.; Lynch, G. C.; Liu, Y. P.; Grarrett, B. C.; Steckler, R.; Issacson, A. D.; Rai, S. N.; Hancock, G. C.; Lauderdale, J. G.; Joseph, T.; Truhlar, D. G. *Comput. Phys. Commun.* **1992**, *71*, 235.
(25) Chuang, Y. Y.; Truhlar, D. G. *J. Chem. Phys.* **2000**, *112*, 1221.
(26) Truhlar, D. G. *J. Comput. Chem.* **1991**, *12*, 266.
(27) Schlegel, H. B.; Sosa, C. *Chem. Phys. Lett.* **1988**, *145*, 329–333.
(28) Ignatyev, I. S.; Xie, Y.; Allen, W. D.; Schaefer, H. F. *J. Chem. Phys.* **1997**, *107*, 141–145.
(29) Young, D. C. *Computational Chemistry: A Practical Guide for Applying Techniques to Real-World Problems*; Wiley-Interscience: New York, 2001; p 227.
(30) Fisher, H.; Radom, L. *Angew. Chem.* **2001**, *113*, 1380.
(31) Kondo, S.; Takahashi, A.; Tokuhashi, K.; Sekiya, A.; Yamada, Y.; Saito, K. *J Fluorine Chem* **2002**, *117*, 47.

(32) (a) Rodgers, A. S.; Chao, J.; Wilhoit, R. C.; Zwolinski, B. J. *J. Phys. Chem. Ref. Data* **1974**, *3*, 117. (b) Frenkel, M.; Kabo, G. J.; Marsh, K. N.; Roganov, G. N.; Wilhoit, R. C. *Thermodynamics of Organic Compounds in the Gas State*; Thermodynamics Research Center: College Station, TX, 1994; Vol. I. (c) Chen, S. S.; Rodgers, A. S.; Chao, J.; Wilhoit, R. C.; Zwolinski, B. J. *J. Phys. Chem. Ref. Data* **1975**, *4*, 441. (d) Cox, J. D.; Wagman, D. D.; Medvedev, V. A. *CODATA Key Values for Thermodynamics*; Hemisphere Publishing Corp.: New York, 1989. (e) Gurvich, L. V.; Veyts, I. V.; Alcock, C. B. *Thermodynamic Properties of Individual Substances*, 4th ed.; Hemisphere Publishing Corp.: New York, 1991; Vol. 2. (f) Rodgers, A. S.; Chao, J.; Wilhoit, R. C.; Zwolinski, B. J. *J. Phys. Chem. Ref. Data* **1974**, *3*, 117.

(33) Kraka, E.; Dunning, T. H., Jr. *Advances in Molecular Electronic Structure Theory*; Dunning, T. H., Jr., Ed.; JAI Press: Stamford, CT, 1990; Vol. 1, p 938.

JP9006262